

Article

Variability of Summer Precipitation Events Associated with Tropical Cyclones over Mid-Lower Reaches of Yangtze River Basin: Role of the El Niño–Southern Oscillation

Fuqiang Cao ^{1,2}, Tao Gao ^{3,4,*} , Li Dan ², Lian Xie ⁵ and Xiang Gong ⁶

¹ School of Geosciences, Shanxi Normal University, Linfen 041000, China; wq2006126@126.com

² CAS Key Laboratory of Regional Climate-Environment Research for Temperate East Asia, Institute of Atmospheric Physics, Chinese Academy of Sciences, Beijing 100864, China; danli@tea.ac.cn

³ College of Urban Construction, Heze University, Heze 274000, China

⁴ State Key Laboratory of Numerical Modeling for Atmospheric Sciences and Geophysical Fluid Dynamics, Institute of Atmospheric Physics, Chinese Academy of Sciences, Beijing 100029, China

⁵ Department of Marine, Earth, and Atmospheric Sciences, North Carolina State University, Raleigh, NC 27607, USA; xie@ncsu.edu

⁶ School of Mathematics and Physics, Qingdao University of Science and Technology, Qingdao 266061, China; gongxiang@qust.edu.cn

* Correspondence: tgao.oc@gmail.com

Received: 29 March 2019; Accepted: 30 April 2019; Published: 9 May 2019



Abstract: Based on tropical cyclone (TC) track data and gridded observational rainfall data of CN05.1 during the period of 1961 to 2014, we examine the contribution of TCs on three metrics of summertime rainfall regimes and identify the connection between TC-induced precipitation events and El Niño–Southern Oscillation (ENSO) in middle–lower reaches of Yangtze River Basin (MLYRB). At the regional scale, TCs are responsible for approximately 14.4%, 12.5%, and 6.9% of rainfall events for normal, 75th, and 95th percentile precipitation cases, respectively. There is no evidence of significant long-term trends of the three type events linked with TCs, while their interdecadal variability is remarkable. Fractionally, larger proportions of TC-induced events occur along southeast coastal regions of MLYRB for normal rainfall events, and they are recorded over southwest and central-east MLYRB for 95th percentile cases. Moreover, a larger contribution of 95th percentile precipitation events to summer total rainfall is found than that for 75th percentile cases, suggesting that TCs may exert stronger impacts on the upper tail of summertime precipitation distribution across MLYRB. The TC-induced normal rainfall events tend to occur more frequency over central-west MLYRB during negative phase of ENSO in summer. However, the higher likelihood of TC-induced rainfall for three defined metrics are found over the majority of areas over MLYRB during negative ENSO phase in spring. In preceding winter, La Niña episode plays a crucial role in controlling the frequency of both normal and 75th percentile precipitation events.

Keywords: extreme rainfall; tropical cyclone; Poisson regression; El Niño–Southern Oscillation

1. Introduction

Tropical cyclones (TCs), which are highly energetic tropical systems, usually trigger weather extremes, such as intense precipitation events, which result in a large number of human fatalities and huge socioeconomic damages [1–4]. In a warming climate, the intensity of extreme TCs is expected to be enhanced. Recent studies argued that the increases and decreases in the frequency of TCs are inhomogeneous at the global-scale, derived from the results of observational analyses and

model simulations [5–7]. Therefore, heavy precipitation events associated with TCs have received much attention (e.g., Mendelsohn et al., 2012; Kossin et al., 2016; Zhang et al., 2018 [8–10]). TCs usually contribute to heavy or extreme rainfall along their paths, and the majority of TC-induced hazards are caused by precipitation extremes and subsequent landslides as well as flash floods [2,4]. Khouakhi et al. [11] investigated the contribution of TCs to extreme precipitation at the global-scale, and pointed out that the TC-induced heavy precipitation events are mainly located along coastal areas; the quantitative contribution of TCs to rainfall variations is ~35–50% over coastal regions at the global-scale.

China, located on the west flank of the Pacific, has a long coastline and has become more vulnerable to landfalling TC activities [10,12,13]: the density of the TC tracks is higher and the number of landfalling TCs is larger during last decades, with more TC-driven precipitation extremes over inland areas [14–16]. Moreover, the western North Pacific (WNP) tends to generate the most and strongest TCs over the world. Recent studies have been conducted to quantify the contribution of TC-induced rainfall during summer (June–August, JJA) in China. Rodgers et al. [17] first found that ~12% of summer rainfall in the WNP was contributed by TCs. Lau et al. [18] emphasized that TCs were responsible for increases in precipitation extremes over the WNP. Chang et al. [19] further revealed the important role of the TC-induced precipitation in shaping the trends of extreme rainfall events over China. Li and Zhou [15] suggested that the TC-induced precipitation accounted for approximately 20–50% of summertime total rainfall over southeast China, and their interdecadal variations during the late 1970s and early 1990s were associated with two regime shifts of total rainfall over southeast coastal areas. By comparing the TC-driven precipitation extremes (within 500 km from TC centers) with the extreme rainfall induced by mesoscale and synoptic systems (beyond 1000 km from TC centers), Zhang et al. [10] indicated that the remarkable influence of TCs on extreme precipitation events is mainly confined to coastal regions in China, which is generally in line with the analyses conducted by Khouakhi et al. [11] at the global-scale.

Furthermore, the spatiotemporal distribution of TC-induced precipitation events is closely linked with trace and tracks of TC activities [20], which is further subject to thermodynamic and dynamic controls over tropical oceans near coastal regions [21]. A burgeoning number of studies demonstrated that the occurrence of intense TC-induced precipitation events is significantly modulated by El Niño–Southern Oscillation (ENSO) across the globe (e.g., Camargo et al., 2007; Colbert et al., 2015; Khouakhi et al., 2017 [11,22,23]). Wang et al. [24,25] demonstrated that the TC activities over the WNP are affected by strong ENSO episodes. In China, inland areas are more influenced by TC-driven precipitation extremes during neutral years than in La Niña or El Niño years [10].

The middle and lower reaches of Yangtze River Basin (MLYRB), with developed economies and urbanization, is situated over the East Asian monsoon region and is also influenced by TCs. The majority of floods over MLYRB derived from extreme rainfall is concentrated in summer [26–28], particularly, MLYRB is more vulnerable to the short-duration extreme precipitation events in rainy season, which is usually responsible for flash flooding [29]. Furthermore, flash floods may be especially deadly since an enormous amount of water falls on saturated ground in a short time across MLYRB. However, the efficient emergency responses are lacked in recent decades because of limitation of sufficient warnings for summertime short-duration precipitation extremes, exacerbating the disastrous effects of these events in MLYRB. In this study, a newly defined index of extreme precipitation events is employed to investigate the frequency and magnitude of summertime short-lived precipitation events affected by TCs over MLYRB within the region 28°–33.5° N, 113°–122° E. A high-resolution dataset is used to calculate the precipitation indices, this dataset has been proved to perform better in characterizing extreme precipitation variability compared to other globally gridded rainfall datasets in China [11,30,31]. The connection between ENSO and TC-induced precipitation extremes was also detected. The rest of text is organized as follows. Section 2 introduces the data and methods. The results are described in Section 3, followed by the discussion and conclusion in Section 4.

2. Data and Methods

We use observational daily rainfall data from the gridded dataset of CN05.1 between 1961 and 2014 [28]. This dataset is constructed based on an interpolation by utilizing more than 2400 observation stations over China, with a high resolution of $0.25^\circ \times 0.25^\circ$. This high-resolution gridding dataset perform better to characterize variability of precipitation extremes over eastern China than other gridded and reanalysis dataset [11,31]. The TC data is obtained from Regional Specialized Meteorological Center (RSMC) Tokyo-Typhoon Center (<http://www.jma.go.jp/jma/indexe.html>). We focus on the TC tracks over the Northwestern Pacific in boreal summer from 1961 to 2014, which are consistent with the period of the observed rainfall dataset. We should keep in mind that the percentage of TC-related extreme events has a strong dependency on the methodology used to define the precipitation extremes and TCs [10,32]. In this study, we follow the method proposed by Kunkel et al. [32], and define a summertime precipitation event that is influenced by a TC when a storm listed in the “best track” cyclone database is within 5° latitude and/or longitude radius (approximately 500 km) for the locations of rainfall events on the same day. This methodology has been widely adopted to examine the variability of TC-induced rainfall studies (e.g., Khouakhi et al., 2017; Aryal et al., 2018; Zhang et al., 2018 [10,11,33]). The Mann–Kendall test for a trend and Sen’s slope estimates are used to estimate and detect linear trends for regional precipitation series (Sen, 1968). Sen’s robust slope estimator based on Kendall’s τ has been widely employed to investigate regional precipitation and temperature changes (e.g., Gao and Wang, 2017 [34]).

In addition, the emergence of TCs with the path passing through regions can trigger different magnitudes of precipitation intensities (e.g., Peduzzi et al., 2012; Khouakhi et al., 2017; Zhang et al., 2018 [2,10,11]), therefore, we focus on three metrics of precipitation regimes to investigate the impacts of TCs on summertime rainfall across MLYRB comprehensively. The 75th and 95th percentiles are applied to define short-lived extreme precipitation events in this study, and we use a range of ± 5 percentile units (75th ± 5 percentile and 95th ± 5 percentile) of selected rainfall values to ensure that all the obtained events are nonoverlapping. Moreover, a 2-week window is utilized around each date of defined events of \pm week (before and after the day with the selected short-lived extreme precipitation events), which guarantees that only the largest precipitation is retained for analyses; others are therefore no longer considered [35,36]. The selected rainfall events using these methods are so-called short-lived extreme precipitation events in comparison with persistent precipitation extremes [37,38]. The TC-induced rainfall events that are less than the threshold of 70th percentile (namely, normal precipitation events) are also taken into account to synthetically examine the influence of TC activities on summertime precipitation events over MLYRB.

Poisson regression is used to examine the dependence of TC-driven precipitation days on ENSO states, in which the TC-induced rainfall days N_i are modeled by a conditional Poisson regression distribution:

$$P(N_i|\lambda_i) = \frac{e^{-\lambda_i} \lambda_i^k}{k!} \quad (k = 0, 1, 2, \dots) \quad (1)$$

where the rate of occurrence λ_i is a nonnegative random variable. We model λ_i as a linear function of the covariate through a logarithmic link function as follows

$$\lambda_i = \exp[\beta_0 + \beta_1 x_1] \quad (2)$$

where β_0 and β_1 are two parameters and x is the covariate of Niño-3.4 index averaged for every season; the Niño-3.4 index time series is available since 1950 from Climate Prediction Center (http://www.cpc.ncep.noaa.gov/products/analysis_monitoring/ensostuff/ensoyears.shtml).

3. Results

3.1. Time Series of TC Rainfall

We adopt three metrics of rainfall regimes to analyze in-depth the contribution of TCs to precipitation events in MLYRB (Figure 1). Normal rainfall events are defined with the daily precipitation being greater than or equal to 1 mm, but excluding the other two kinds of short-lived precipitation extremes at the 75th and 95th percentile cases. Based on these definitions, the number of precipitation events over MLYRB caused by TCs in summer from 1961 to 2014 is 546, 44, and 24 for the normal, 75th, and 95th percentile precipitation events, respectively. In general, the proportional contributions of the frequency of TC-induced rainfall to the number of total precipitation events are not apparent, with the strongest contribution up to 14.4% for normal rainfall events, and fewer extreme precipitation events originate from TCs. The rainfall amount of normal events is roughly 2–3 times that of the 75th and 95th percentile cases (black lines in Figure 1a,c,e). While the rainfall accumulation of TC-induced events also exhibits distinct discrepancies among three defined precipitation regimes (blue lines in Figure 1a,c,e). A similar phenomenon is also recorded for the time series of number of precipitation events (Figure 1b,d,f).

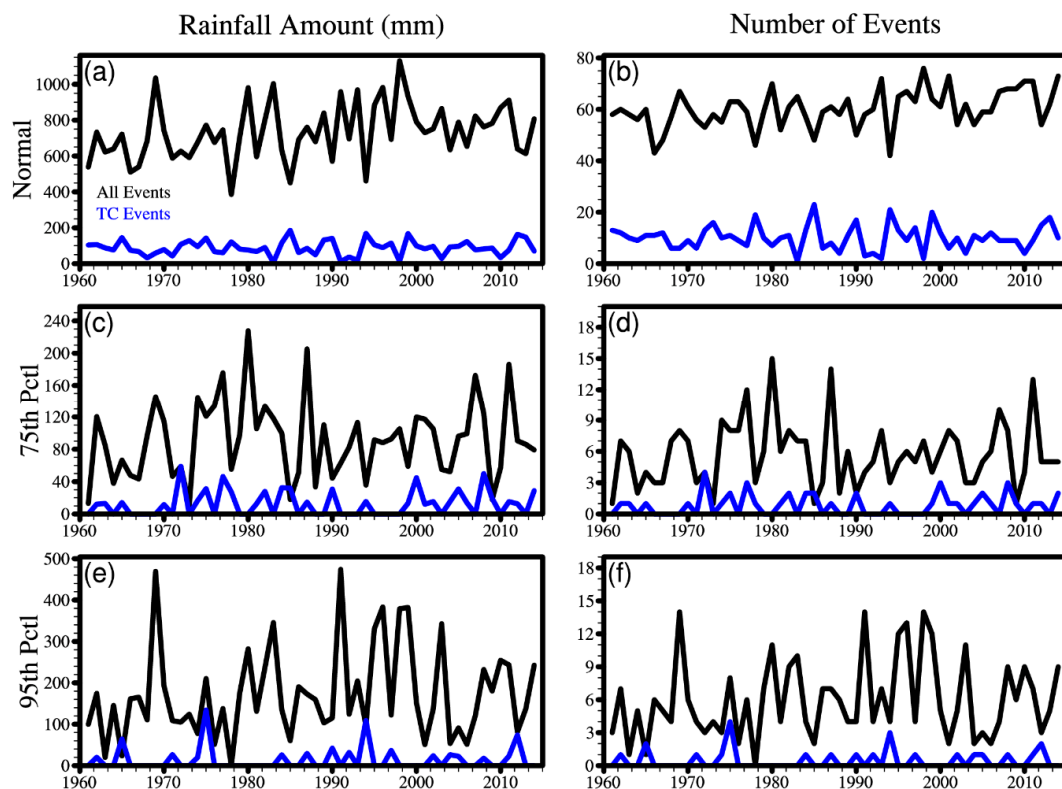


Figure 1. (a) Time series of the amount of total and TC-induced normal rainfall events over the middle–lower reaches of the Yangtze River (MLYRB) during summer. (b) Time series of the number of total and TC-induced normal rainfall events. (c) and (d) are the same as (a) and (b), but for 75th percentile precipitation events. (e) and (f) are the same as (a) and (b), but for 95th percentile precipitation events.

The trends of extreme non-TC rainfall frequency are not significant (Figure 1d,f), with slightly increasing trends of 0.1 and 0.4 per decade at the 75th and 95th precipitation events, respectively. Nevertheless, time series of normal non-TC event frequency exhibit a statistically significant increasing trend of 1.9 per decade (Figure 1b), while the corresponding TC-induced rainfall events display a slightly declining trend, without exceeding the 95% confidence level. Similarly, linear trends of

the time series of the TC-induced precipitation events are also inconspicuous. Particularly for 75th and 95th percentile events, there are not enough number of events linked to TCs for fitting linear trend during the entire period. However, the interdecadal variability is remarkable both for non-TC precipitation events and the extremes derived from TC activities. For the 75th percentile precipitation events, most of the TC-induced events occurred during the period of 1970 to 1990 and after 2000, while the extreme events caused by TCs are more concentrated around the 1990s and 2010s at the 95th percentile events (Figure 1d,f). Moreover, few TC-induced extreme events appear from mid-1960s to 1970, and around 1990s at the 75th percentile events, whereas there exist no extreme events linked to TCs from the mid-1960s to 1970, and around the 1980s and 2000s for the period 1961 to 2014 for 95th percentile cases. These are possibly subjected to time series of TC-related rainfall exhibiting remarkable interdecadal shifts, with potential change points identified around the late 1970s and 1990s [15,39]. Pronounced variability of normal non-TC rainfall events are also found from 1970 to 2000 (Figure 1b), even though the number of events is relatively larger during the entire period in comparison with ones for 75th and 95th percentile cases. Additionally, changes in TC-induced precipitation amount over time are not consistent with that of total rainfall (Figure 1a,c,e), the possible cause may be that the percentage of TC-induced precipitation events is not large compared with total rainfall events. Furthermore, there are also some years that have high total accumulated precipitation from extreme events without any TC (e.g., 1968 and 1980 for 75th percentile cases, and 1969 and 1999 for the 95th cases). Overall, no statistically adequate evidence suggests that the TCs are significantly responsible for variations in extreme precipitation events over MLYRB during 1961–2014, in particular for short-lived precipitation extremes. The possible reason for this phenomenon is that MLYRB receives much monsoonal precipitation in summer, which, to a certain degree, results in less contribution of TC-induced events to summer total rainfall [40–42].

3.2. TC Tracks and Spatial Distribution of TC Rainfall

Existing studies have documented that the frequency and magnitude of precipitation events derived from TCs can be attributed to variations of TC tracks (e.g., Corporal-Lodangco et al., 2016 [20]). Therefore, the TC tracks at multiple time scales are analyzed in this study to facilitate a better understanding of the variability of TC-induced rainfall events. Figure 2 shows the TC tracks located over the WNP from 1961 to 2014. The spatial distribution of annual total TC tracks suggests that the regions affected by TC activities are mainly expansive over central-east China and southeast China (Figure 2a). The majority of TCs exhibit straight-moving tracks and enter landward regions, whereas a small portion of TCs with recurring tracks extending farther northeast, even at higher latitudes, which provide favorable conditions to produce TC-induced precipitation events over inland areas. In summer, the number of landfalling TC tracks decreases significantly compared to annual ones (Figure 2a,b), since a considerable number of TCs that impact the rainfall events in China occurs in autumn, with few of them appearing in winter [15,42]. Moreover, not all TCs can cause rainfall events across MLYRB in summer as the number of TCs related to precipitation events over MLYRB declines distinctly compared to all the summertime TCs (Figure 2b,c). Figure 2b exhibits that a larger number of summertime TCs do not make landfall over inland China, since their tracks are principally limited over the WNP (Figure 2b) and cannot trigger precipitation events in MLYRB. The strength of the landfalling TCs, inducing those linked to normal rainfall events, is relatively weak over MLYRB (Figure 2d), nevertheless, some high-intensity TCs passing through the MLYRB account for both 75th and 95th percentile rainfall events (Figure 2e,f), indicating that enhanced TCs may generate short-lived extreme precipitation events over MLYRB. Furthermore, the number of TC tracks at the 75th percentile cases are more than that for 95th percentile events, consistent with more regional 75th percentile events than 95th cases.

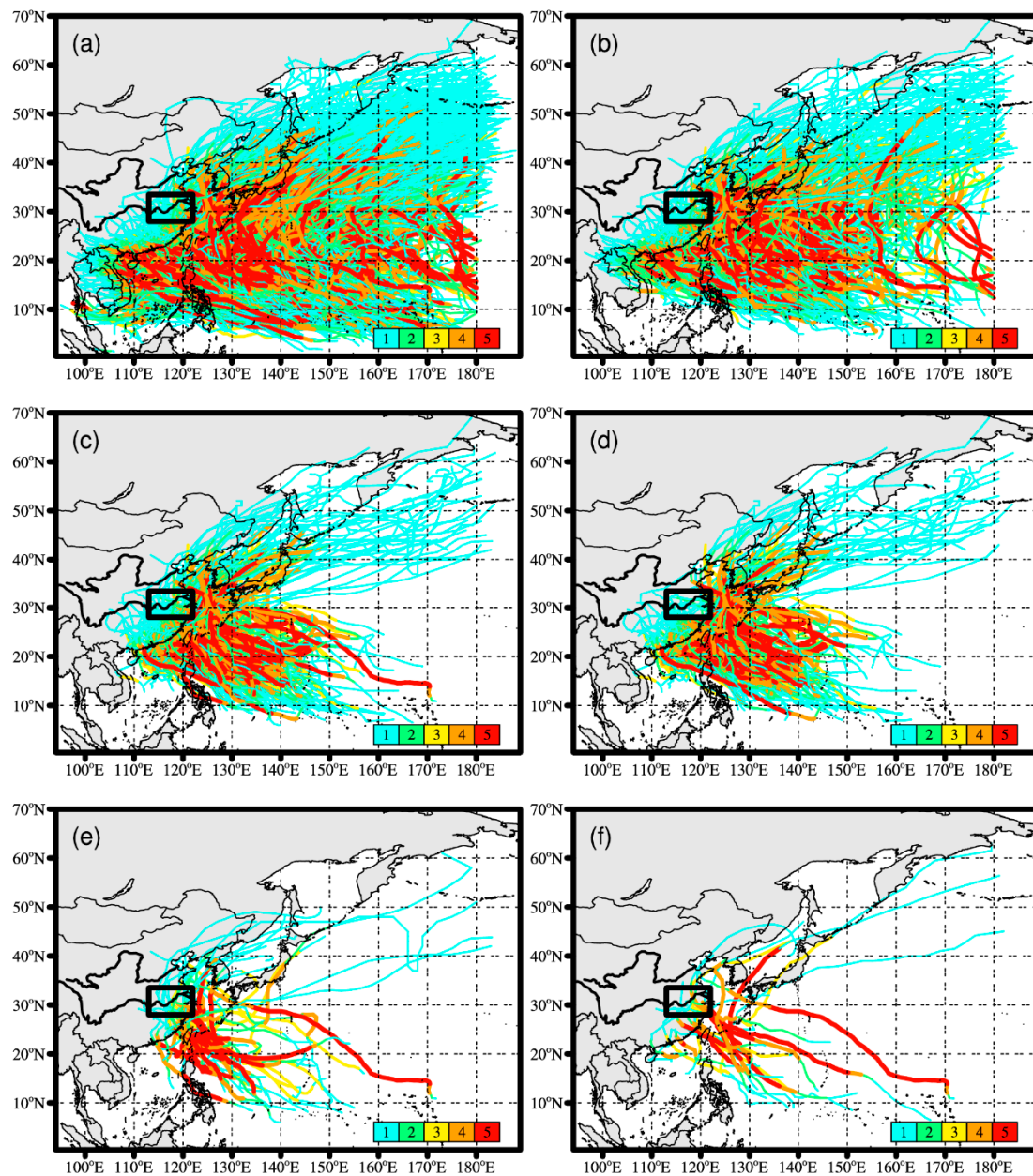


Figure 2. The observational TC tracks between 1961 and 2014. The color scales denote Saffir–Simpson hurricane wind scales. (a) All the annual TC tracks. (b) Summertime TC tracks. (c) All TC tracks that induce precipitation in summer. (d) The TC tracks that induce normal rainfall events in summer. (e,f) The TC tracks that induce 75th and 95th percentile precipitation events, respectively. The black rectangle denotes the middle–lower reaches of Yangtze River Basin (MLYRB) within the region 28° – 33.5° N, 113° – 122° E.

In addition to regional TC-induced rainfall events, as shown in Figure 1, we also calculate the number and amount of TC-induced precipitation events at each gridded site scale to further investigate spatial distribution of TC contributions to summer total rainfall. Larger summer mean non-TC rainfall is mainly located over central-south and eastern MLYRB, and the number of corresponding events exceeds 24 in some regions (Figure S1a). For normal TC-induced rainfall events, larger summer mean precipitation amount is primarily situated over southeast, southwest and central MLYRB (Figure 3b), with summer mean TC-induced precipitation in excess of 20 mm, this roughly coincides with corresponding TC tracks shown in Figure 2d. It can be seen that the TC-tracks passing through

MLYRB are primarily concentrated over central-south MLYRB, providing suitable conditions for the occurrence of precipitation events. Figure 3c illustrates the relative contribution of TC-induced precipitation to summer total rainfall amount. The largest contributions are found over southeast MLYRB, which is consistent with the location of larger summer mean TC-induced rainfall. While the central and southwest MLYRB has larger summer mean TC-induced rainfall, demonstrating insignificant spatial coherence (Figure 3b,c). For the non-TC precipitation events at the 75th percentile events, southern MLYRB exhibits relatively larger summer mean rainfall amounts, whereas the number of events is less than that for every year (Figure S1d). The larger summer mean TC-induced rainfall concentrates in central-east MLYRB (Figure 3e), where the summer mean non-TC rainfall is small. The larger contribution of TC-induced precipitation to summer total rainfall is located over northeast MLYRB (Figure 3f). Overall, the number and amount of TC-induced precipitation events and their contribution to summer total rainfall for 75th percentile cases are not conspicuous at spatial scale. The homogeneous distribution of non-TC and TC-induced rainfall is remarkable at the 95th percentile precipitation events (Figure 3g,h,i). For the non-TC events, larger summer mean rainfall is mainly distributed over central-west areas, with amounts up to 280 mm (Figure 3g). In contrast, the larger TC-induced precipitation amount is situated over central-east regions (Figure 3h), which is consistent with the distribution of contributions of that to summer total rainfall (Figure 3i) and major TC tracks passing through the MLYRB (Figure 2i).

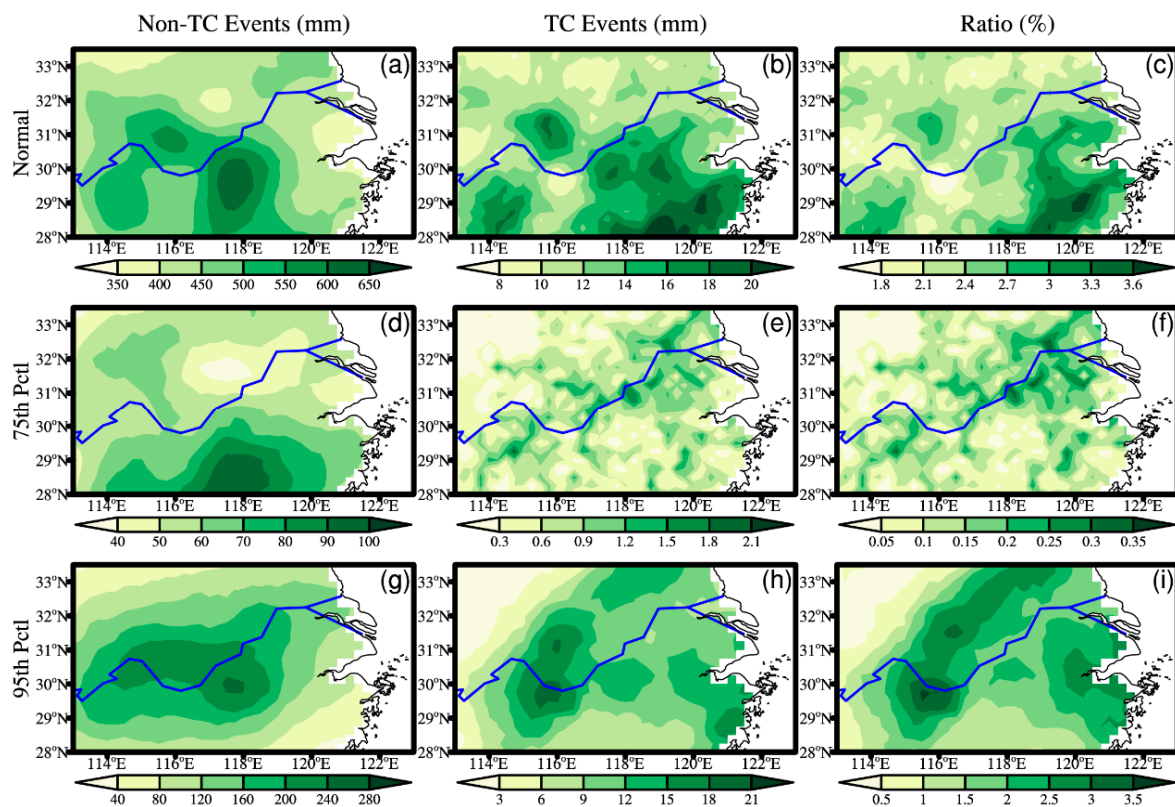


Figure 3. (a–c) Spatial distribution of the summer mean non-TC rainfall and TC-induced rainfall as well as relative contribution of TC-induced rainfall to the summer mean rainfall for normal precipitation events, respectively, shade denotes the rainfall amount and curve denotes the number of precipitation events. (d–f) The same as a–c, but for 75th percentile precipitation events. (g–i) The same as (a–c), but for 95th percentile precipitation events. The bold blue curve denotes the Yangtze River.

In general, the contribution of TC-induced precipitation events to summer total rainfall is not significant across MLYRB, with the largest fractional contribution accounting for approximately 3.6% for normal and 95th percentile precipitation events. However, the contribution of 75th percentile cases is one order of magnitude smaller than that for normal and 95th percentile events, the possible cause may be that the number of 75th percentile precipitation events is less than normal events at spatial scale, combined to the rainfall intensity being weaker than 95th percentile events at each gridded site. Additionally, the precipitation extremes are often defined using a threshold or return period in previous studies [11,33,42], which does not change along with time of year, thereby influencing the discrepancy of the number of extreme precipitation events affected by TCs in comparison with results in this study.

3.3. Extreme TC Precipitation and ENSO

Since a large number of studies have indicated that the TC activities are modulated by different phases of ENSO episodes (e.g., Camargo et al., 2007; Colbert et al., 2015; Khouakhi et al., 2017; Zhang et al., 2018 [10,11,22,23]). To examine the relationship between ENSO and TC-induced precipitation events comprehensively, we focus on three seasonal Niño-3.4 indices during summer, spring (March–May (MAM)), and the preceding winter (December, January, and February (DJF)) for analyzing the influences of ENSO on TC-induced rainfall over MLYRB. Figure 4 summarizes the outcomes from Poisson regression exhibiting the role of ENSO to occurrence of the TC-induced precipitation events at different levels of significance, in which we focus on summer Niño-3.4 index. Each grid shows the estimated value of the β_1 coefficient derived from Poisson regression (Equation (2)); negative values (red) denote a greater probability of the TC-induced rainfall events during negative phase of ENSO, conversely, positive values (blue) denote a greater probability of the events during positive phase of ENSO. Figure 4a highlights the spatial geographical difference of the relationship between normal TC-induced rainfall events and ENSO, with normal events occurring in different ENSO phases. Particularly, the spatially coherent negative signals, with significance at 5% and 10% levels, are found over central-west MLYRB and the majority of northern areas, suggesting that normal TC-induced rainfall events occur with a greater probability during negative ENSO phase. On the contrary, over southeast and northeast MLYRB we found a positive connection with ENSO with significance at 5% and 10% levels, indicating that the normal TC-induced rainfall events are more likely during positive phases of ENSO. Overall, the impact of negative ENSO phases is more significant over the majority of regions across MLYRB. However, spatially coherent positive signals are dominated over most of areas for 75th and 95th percentile precipitation events, even though not exceeding the 95% confidence level (Figure 4b,c), there are also suggestions indicating that we may generally expect more TC-induced short-lived extreme precipitation events during positive ENSO phases. Only few gridded sites located northeast and southeast show negative values of the coefficient for 75th percentile events, where the short-lived precipitation extremes are generally tied to occurrence of the WNP TCs during negative phases of ENSO. For the 95th percentile cases, very few gridded sites with negative coefficient are sporadically distributed in northwest MLYRB, implying a higher likelihood of short-lived extreme precipitation events caused by TCs during negative ENSO phases. The above analyses suggest that there are remarkable discrepancies between the impacts of ENSO on normal rainfall events and short-lived precipitation extremes caused by TCs over MLYRB in summer, we expect a greater probability of occurrence of normal (extreme) short-lived rainfall events associated with WNP TCs during negative (positive) phases of ENSO.

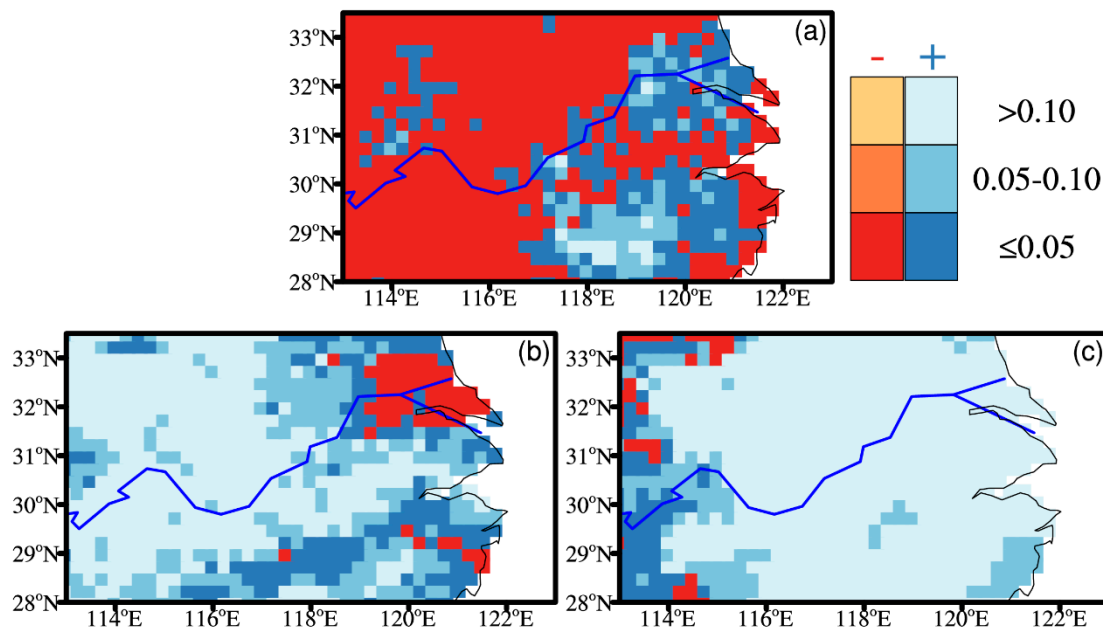


Figure 4. Relationship between summertime precipitation events associated with tropical cyclones (TCs) and El Niño–Southern Oscillation (ENSO), regression coefficients derived from Poisson regression display at different level of significance. (a) Normal rainfall events. (b) 75th percentile precipitation events. (c) 95th percentile precipitation events. The bold blue curve denotes the Yangtze River.

In spring, the connection between ENSO and TC-induced rainfall events is even stronger (Figure 5) compared to those during summer. The coherent negative signals with significance at 5% level are seen at all of the gridded sites for normal rainfall events caused by TCs (Figure 5a), suggesting that the TCs are more likely to produce normal events during the negative phases of spring ENSO. Furthermore, we also found a higher number of gridded sites having negative coefficients with significance at the 5% level for both the 75th and 95th percentile precipitation events (Figure 5b,c), indicating that the frequency of short-lived precipitation extremes caused by TCs is larger during negative ENSO phases in spring. Generally, the frequency of the three kinds of TC-induced rainfall events tend to increase in spring during negative ENSO phases over MLYRB. In the preceding winter, the influences of ENSO on TC-induced rainfall events are evidently different among three kinds of defined precipitation events (Figure 6). The negative relationship with ENSO is found over southeast, central, and northern MLYRB for normal rainfall events (Figure 6a), where we expect a larger number of normal events associated with TCs during La Niña years in preceding winter. While the connection between ENSO and short-lived precipitation extremes is even stronger when considering 75th percentile precipitation events (Figure 6b), almost all of gridded sites exhibit a negative coefficient, suggesting a higher likelihood of 75th percentile events during preceding winter La Niña years. However, the impact of ENSO on 95th percentile precipitation events linked with TCs is insignificant (Figure 6c), only few gridded sites with significant coefficient are limited over northwest and southern MLYRB. These sites indicate that in the preceding winter La Niña play a pronounced role on the occurrence of normal and moderate (75th) TC-induced rainfall events, rather than short-lived precipitation extremes (95th percentile rainfall events). Our findings of the relationship between precipitation regimes and ENSO in preceding spring and winter are generally consistent with the studies by Wang et al [24,25].

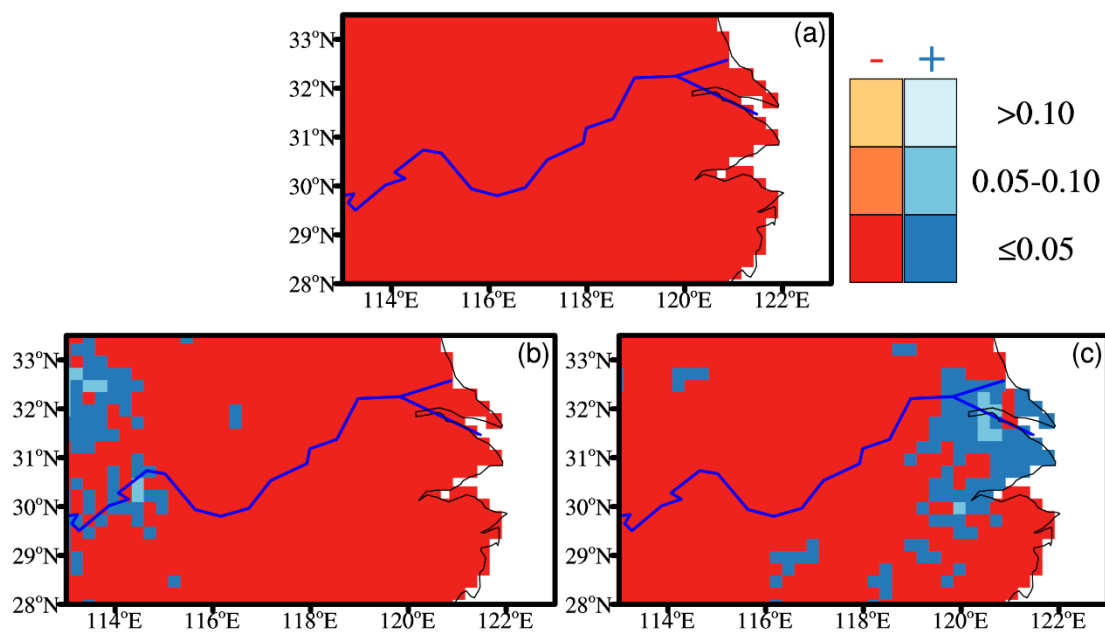


Figure 5. Relationship between summertime precipitation events associated with tropical cyclones (TCs) and El Niño–Southern Oscillation (ENSO) in spring, regression coefficients derived from Poisson regression display at different level of significance. (a) Normal rainfall events. (b) 75th percentile precipitation events. (c) 95th percentile precipitation events. The bold blue curve denotes the Yangtze River.

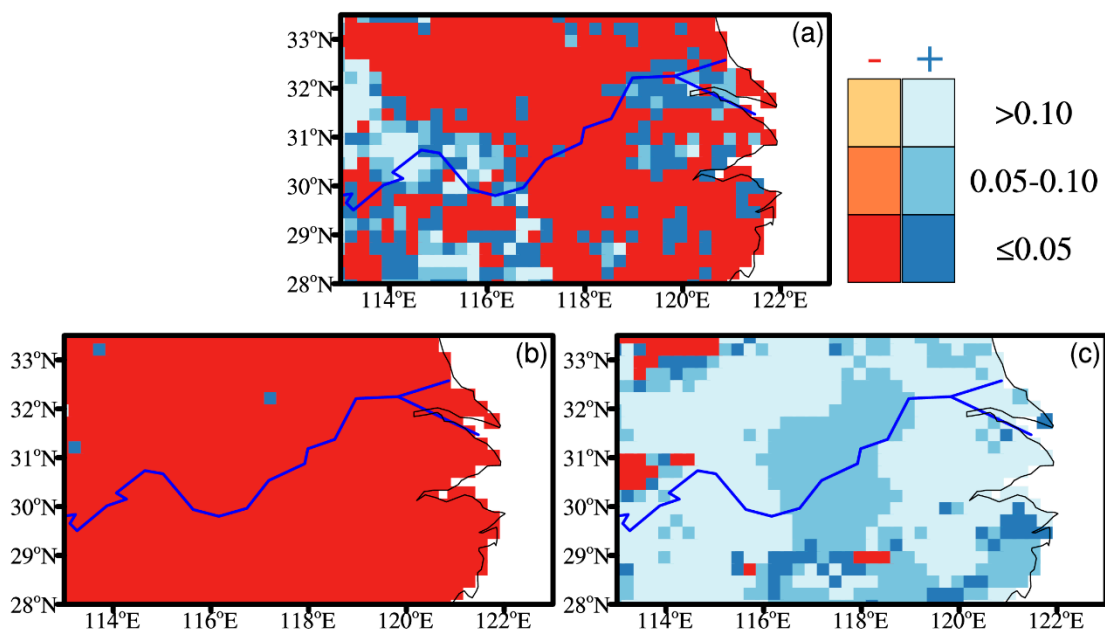


Figure 6. Relationship between summertime precipitation events associated with tropical cyclones (TCs) and El Niño–Southern Oscillation (ENSO) in preceding winter, regression coefficients derived from Poisson regression display at different level of significance. (a) Normal rainfall events. (b) 75th percentile precipitation events. (c) 95th percentile precipitation events. The bold blue curve denotes the Yangtze River.

Previous studies suggested that there is a spatial pattern shift of El Niño from the Eastern Pacific type to the Central Pacific type since 1990s [43,44]. To obtain a comprehensive understanding of the influences of ENSO on summertime precipitation regimes across MLYRB, we also analyzed the

connections between summertime precipitation events and Niño 3 and Niño 4 indices (Figures S2–S7). The obvious differences of the results derived from Niño-3.4 and Niño 3 are seen in preceding spring and winter. The positive phases of ENSO have a greater impact on short-lived precipitation extremes for 95th percentile cases over central-east regions (Figure S3c) in spring. While the evident difference is recorded for normal rainfall in preceding winter (Figure S4a), the influences of negative phases of ENSO on normal precipitation events is relatively weaker compared to that of Niño-3.4. However, the regression results of Niño 4 are roughly similar to that of Niño-3.4, only minor differences occur for short-lived extreme precipitation events at the 75th percentile cases in summer (Figure S5b) and 95th percentile cases in preceding winter (Figure S7c). Overall, the analyses of Niño 3 and Niño 4 indices further confirmed the results from the Niño-3.4 index. Additionally, we also investigate the impacts of Philippine Sea anticyclone [45,46] in preceding winter on summertime precipitation regimes in MLYRB (Figure S8). The regression results are different with ENSO index, the underlying causes will form our forthcoming studies.

4. Discussion and Conclusions

Using an observational gridded rainfall dataset and TC track dataset, we provide a comprehensive analysis focusing on influences of TCs on summertime rainfall over MLYRB between 1961 and 2014. Two types of defined short-lived extreme precipitation events are employed; meanwhile, a normal TC-induced rainfall event is also utilized to further compare the characteristics of short-lived precipitation extremes.

At the regional scale, there are more TC-related events for normal rainfall (546 out of 3794) than that for 75th (44 out of 353) and 95th (24 out of 347) percentile precipitation, implying that the impact of TCs on nonextreme rainfall events is even more significant than ones of short-lived precipitation extremes (75th and 95th). These small fractional proportions are not necessarily believed that TCs are not contributing to variations in summertime precipitation extremes in MLYRB, since the time series of three kinds of TC-induced rainfall events show remarkable interdecadal variability, with differently potential shift points of TC-induced rainfall events for three metrics of precipitation regimes (Figure 1). While the linear trends of TC-induced precipitation events and non-TC events are not significant, except for non-TC normal events with statistically significant increasing trend of 1.9 per decade.

The spatial distribution of annual total TC tracks indicates that MLYRB is not the most affected region by TCs in China; consistent findings are also reported by Li and Zhou [15] and Li et al. [47], who pointed out that in TC-affected regions the contribution of TC-related precipitation to total rainfall reaches up to 50%, and was chiefly distributed in southeast coastal regions and Hainan, rather than concentrated across MLYRB. Furthermore, the considerable proportion of TCs originated from WNP cannot trigger rainfall events over MLYRB in summer, as their tracks are mainly limited over WNP and they do not make landfall across MLYRB (Figure 2b,c). There are more strengthened landfalling TCs passing through the MLYRB at the both 75th and 95th percentile events compared to that for normal rainfall events (Figure 2d–f). These TCs tracks exert a control on the spatial distribution of the contributions of TC-induced precipitation to summer total rainfall over MLYRB (Figure 3). The distribution of summer mean normal TC-induced rainfall suggests that the highest precipitation amount in excess of 20 mm are mainly found over central, southwest and southeast MLYRB, which is not consistent with corresponding non-TC events with larger rainfall totals exceeding 600 mm situated over central and southwest (Figure 3a,b). For TC-induced precipitation, the highest proportions are recorded along southeast coastal regions of MLYRB (Figure 3c). It is worth noting that the similar relative TC-induced contributions are found at the 95th percentile precipitation events, while the spatial distribution of higher TC-induced rainfall proportions exhibits remarkable discrepancies between normal rainfall events and 95th percentile cases (Figure 3c,i). Moreover, the distribution of TC-induced contributions at the 95th percentile rainfall events roughly coincides with that of mean TC-induced precipitation in summer. However, both of the summer TC-induced rainfall accumulation and proportions for 75th percentile events are much smaller compared to normal and 95th percentile

precipitation events, suggesting that TCs may have stronger influences on the lower and upper tail of precipitation distribution than on the moderate rainfall events (75th percentile events).

Given the connection between TC genesis/tracks and major climate modes, for example ENSO [10,11,20], we examine the relationship between TC-induced rainfall events and ENSO during three seasons. In summer, negative ENSO phases witness a greater probability of normal TC-induced rainfall events over central-west MLYRB, while we would expect more normal events associated with TCs in northeast and southeast areas of MLYRB during positive phases of ENSO. However, the impacts of ENSO on short-lived extreme precipitation events in the 75th and 95th percentile cases are insignificant, and only sporadic gridded sites exhibited positive/negative signals with significance at 5% and 10% levels (Figure 4b,d), implying that ENSO triggers a weak control on the number of short-lived precipitation extremes affected by TCs over MLYRB in summer. On the contrary, an increased probability of TC-induced events is found during negative ENSO phases for three kinds of defined precipitation indices in spring (Figure 5). Nevertheless, the influences of ENSO on TC-induced rainfall events in preceding winter are more complex in comparison with that in spring and summer. The negative relationship with ENSO, exceeding the significance at the 5% level, is found at the majority of gridded sites for normal events and almost all of the sites for 75th percentile precipitation events, suggesting that a higher likelihood of TC-induced events for these two kinds of defined precipitation events during La Niña years. While the impacts of ENSO on 95th percentile precipitation events are not significant, with few gridded sites having significantly positive (negative) signals with significance at 5% level (Figure 6). These are consistent with the spatial pattern of the corresponding values of β_0 and β_1 in preceding winter (Figure S9).

In general, our results suggest that TCs play a minor role (approximately 3.6%) in determining summer rainfall budget over MLYRB between 1961 and 2014. This may be because that MLYRB is located in monsoonal regions and receives considerable monsoonal rainfall amount [44–46]. Moreover, precipitation over MLYRB is also affected by local forcing factors, for example orographic landscape features (e.g., Yu and Kao, 2007; You et al., 2009; Miao et al., 2016; Kendon et al., 2018 [46,48–50]). However, TC-induced short-lived extreme precipitation events across MLYRB in summer often generate devastating consequences in the context of the summertime saturated soil environment [27,43]. The damages derived from TC-induced precipitation events will likely escalate, which is attributed to the increasing populations living in areas affected by TCs (e.g., Mendelsohn et al., 2012 [8]), and the future projection of TC-induced intense rainfall increase up to 20% in a warmer climate (e.g., Knutson et al., 2015 [7]). Note that our findings, to a certain degree, are not comparable to previous studies (e.g., Jiang and Zipser, 2010; Zhang et al., 2018 [42,51]), likely because of the different definition of precipitation extremes and criteria of TCs as well as length of periods used for different analyses. Moreover, the different indices of ENSO that are used for analyses may also affect the discrepancies of results [43–47]. Despite these differences, the connection that has been identified between TC-induced precipitation extremes and ENSO may help predict occurrence of the TC-induced extreme precipitation events where the close linkage between ENSO and TC-driven intense rainfall has been discovered.

Supplementary Materials: The following are available online at <http://www.mdpi.com/2073-4433/10/5/256/s1>, Figure S1: (a), (b) and (c) Spatial distribution of the number of summer non-TC rainfall events and TC-induced rainfall events as well as relative contribution of TC-induced rainfall events to the summer rainfall events for normal precipitation events, respectively, shade denotes the number of precipitation events. (d), (e) and (f) The same as (a), (b) and (c), but for 75th percentile precipitation events. (g), (h) and (i) The same as (a), (b) and (c), but for 95th percentile precipitation events. The bold blue curve denotes the Yangtze River. Figure S2: Relationship between summertime precipitation events associated with TCs and summer Niño 3 index, regression coefficients derived from Poisson regression displayed at different level of significance. (a) Normal rainfall events. (b) 75th percentile precipitation events. (c) 95th percentile precipitation events. The bold blue curve denotes the Yangtze River. Figure S3: The same as Figure S2. But for preceding spring ENSO. Figure S4: The same as Figure S2. But for preceding winter ENSO. Figure S5: Relationship between summertime precipitation events associated with TCs and summer Niño 4 index, regression coefficients derived from Poisson regression displayed at different level of significance. (a) Normal rainfall events. (b) 75th percentile precipitation events. (c) 95th percentile precipitation events. The bold blue curve denotes the Yangtze River. Figure S6: The same as Figure S5. But for preceding spring ENSO. Figure S7: The same as Figure S5. But for preceding winter ENSO. Figure S8: Relationship between

summertime precipitation events associated with TCs and preceding winter Philippine Sea anticyclone (PSAC), regression coefficients derived from Poisson regression displayed at different level of significance. (a) Normal rainfall events. (b) 75th percentile precipitation events. (c) 95th percentile precipitation events. The bold blue curve denotes the Yangtze River. Figure S9: The values of β_0 and β_1 when the Niño-3.4 index is used as covariate of averaged for preceding winter.

Author Contributions: F.C. and T.G.; Methodology, F.C. and T.G.; Formal Analysis, T.G.; Investigation, X.G.; F.C., T.G., and L.D. Writing—Original Draft Preparation, L.X. and X.G.; Writing—Review and Editing.

Funding: This research received no external funding.

Acknowledgments: This study is jointly supported by the Natural Science Foundation and Sci-tech development project of Shandong Province (No. ZR2018MD014; J18KA210), the National Natural Science Foundation of China (Key Program) (No. 41330423, 41630532), Project funded by China Postdoctoral Science Foundation (No. 119100582H; 1191005830), International Partnership Program of Chinese Academy of Sciences (No. 134111KYSB20160031), R&D Special Fund for Public Welfare Industry (meteorology) (No. GYHY201506012).

Conflicts of Interest: The authors declare no conflict of interest.

References

1. Webster, P.J.; Holland, G.J.; Curry, J.A.; Chang, H. Changes in tropical cyclone number, duration, and intensity in a warming environment. *Science* **2005**, *309*, 1844–1846. [[CrossRef](#)] [[PubMed](#)]
2. Peduzzi, P.; Chatenoux, B.; Dao, H.; De Bono, A.; Herold, C.; Kossin, J.; Mouton, F.; Nordbeck, O. Global trends in tropical cyclone risk. *Nat. Clim. Chang.* **2012**, *2*, 289. [[CrossRef](#)]
3. Chen, Y.C.; Chang, K.T.; Chiu, Y.J.; Lau, S.M.; Lee, H.Y. Quantifying rainfall controls on catchment-scale landslide erosion in Taiwan. *Earth Surf. Proc. Landf.* **2013**, *38*, 372–382. [[CrossRef](#)]
4. Czajkowski, J.; Villarini, G.; Michel-Kerjan, E.; Smith, J.A. Determining tropical cyclone inland flooding loss on a large scale through a new flood peak ratio-based methodology. *Environ. Res. Lett.* **2013**, *8*, 44056. [[CrossRef](#)]
5. Tian, F.; Zhou, T.; Zhang, L. Tropical cyclone genesis potential index over the western North Pacific simulated by LASG/IAP AGCM. *Acta Meteorol. Sin.* **2013**, *27*, 50–62. [[CrossRef](#)]
6. Emanuel, K.A. Downscaling CMIP5 climate models shows increased tropical cyclone activity over the 21st century. *Proc. Natl. Acad. Sci. USA* **2013**, *110*, 12219–12224. [[CrossRef](#)]
7. Knutson, T.R.; Sirutis, J.J.; Zhao, M.; Tuleya, R.E.; Bender, M.; Vecchi, G.A.; Villarini, G.; Chavas, D. Global projections of intense tropical cyclone activity for the late twenty-first century from dynamical downscaling of CMIP5/RCP4. 5 scenarios. *J. Clim.* **2015**, *28*, 7203–7224. [[CrossRef](#)]
8. Mendelsohn, R.; Emanuel, K.; Chonabayashi, S.; Bakkensen, L. The impact of climate change on global tropical cyclone damage. *Nat. Clim. Chang.* **2012**, *2*, 205. [[CrossRef](#)]
9. Kossin, J.P.; Emanuel, K.A.; Camargo, S.J. Past and projected changes in western North Pacific tropical cyclone exposure. *J. Clim.* **2016**, *29*, 5725–5739. [[CrossRef](#)]
10. Zhang, Q.; Gu, X.; Li, J.; Shi, P.; Singh, V.P. The impact of tropical cyclones on extreme precipitation over coastal and inland areas of China and its association to ENSO. *J. Clim.* **2018**, *31*, 1865–1880. [[CrossRef](#)]
11. Khouakhi, A.; Villarini, G.; Vecchi, G.A. Contribution of tropical cyclones to rainfall at the global scale. *J. Clim.* **2017**, *30*, 359–372. [[CrossRef](#)]
12. Zhang, Q.; Wu, L.; Liu, Q. Tropical cyclone damages in China 1983–2006. *Bull. Am. Meteorol. Soc.* **2009**, *90*, 489–496. [[CrossRef](#)]
13. He, C.; Wu, B.; Zou, L.; Zhou, T. Responses of the summertime subtropical anticyclones to global warming. *J. Clim.* **2017**, *30*, 6465–6479. [[CrossRef](#)]
14. Ying, M.; Chen, B.; Wu, G. Climate trends in tropical cyclone-induced wind and precipitation over mainland China. *Geophys. Res. Lett.* **2011**, *38*. [[CrossRef](#)]
15. Li, R.C.; Zhou, W. Interdecadal changes in summertime tropical cyclone precipitation over Southeast China during 1960–2009. *J. Clim.* **2015**, *28*, 1494–1509. [[CrossRef](#)]
16. Zhang, W.; Xie, L.; Liu, B.; Guan, C. An Integrated Approach for Assessing Tropical Cyclone Track and Intensity Forecasts. *Weather Forecast.* **2017**, *32*, 969–990. [[CrossRef](#)]
17. Rodgers, E.B.; Adler, R.F.; Pierce, H.F. Contribution of tropical cyclones to the North Pacific climatological rainfall as observed from satellites. *J. Appl. Meteorol.* **2000**, *39*, 1658–1678. [[CrossRef](#)]

18. Lau, K.M.; Zhou, Y.P.; Wu, H.T. Have tropical cyclones been feeding more extreme rainfall? *J. Geophys. Res. Atmos.* **2008**, *113*. [[CrossRef](#)]
19. Chang, C.P.; Lei, Y.; Sui, C.H.; Lin, X.; Ren, F. Tropical cyclone and extreme rainfall trends in East Asian summer monsoon since mid-20th century. *Geophys. Res. Lett.* **2012**, *39*. [[CrossRef](#)]
20. Corporal-Lodangco, I.L.; Leslie, L.M.; Lamb, P.J. Impacts of ENSO on Philippine tropical cyclone activity. *J. Clim.* **2016**, *29*, 1877–1897. [[CrossRef](#)]
21. Chand, S.S.; Tory, K.J.; McBride, J.L.; Wheeler, M.C.; Dare, R.A.; Walsh, K.J. The different impact of positive-neutral and negative-neutral ENSO regimes on Australian tropical cyclones. *J. Clim.* **2013**, *26*, 8008–8016. [[CrossRef](#)]
22. Camargo, S.J.; Emanuel, K.A.; Sobel, A.H. Use of a genesis potential index to diagnose ENSO effects on tropical cyclone genesis. *J. Clim.* **2007**, *20*, 4819–4834. [[CrossRef](#)]
23. Colbert, A.J.; Soden, B.J.; Kirtman, B.P. The impact of natural and anthropogenic climate change on western North Pacific tropical cyclone tracks. *J. Clim.* **2015**, *28*, 1806–1823. [[CrossRef](#)]
24. Wang, B.; Chan, J.C. How strong ENSO events affect tropical storm activity over the western North Pacific. *J. Clim.* **2002**, *15*, 1643–1658. [[CrossRef](#)]
25. Wang, B.; Xiang, B.; Lee, J. Subtropical high predictability establishes a promising way for monsoon and tropical storm predictions. *Proc. Natl. Acad. Sci. USA* **2013**, *110*, 2718–2722. [[CrossRef](#)]
26. Guan, Z.; Han, J.; Li, M. Circulation patterns of regional mean daily precipitation extremes over the middle and lower reaches of the Yangtze River during the boreal summer. *Clim. Res.* **2012**, *50*, 171–185. [[CrossRef](#)]
27. Gao, T.; Xie, L.; Liu, B. Association of extreme precipitation over the Yangtze River Basin with global air–sea heat fluxes and moisture transport. *Int. J. Climatol.* **2016**, *36*, 3020–3038. [[CrossRef](#)]
28. Li, C.; Tian, Q.; Yu, R.; Zhou, B.; Xia, J.; Burke, C.; Dong, B.; Tett, S.F.; Freychet, N.; Lott, F. Attribution of extreme precipitation in the lower reaches of the Yangtze River during May 2016. *Environ. Res. Lett.* **2018**, *13*, 14015. [[CrossRef](#)]
29. Westra, S.; Fowler, H.J.; Evans, J.P.; Alexander, L.V.; Berg, P.; Johnson, F.; Kendon, E.J.; Lenderink, G.; Roberts, N.M. Future changes to the intensity and frequency of short-duration extreme rainfall. *Rev. Geophys.* **2014**, *52*, 522–555. [[CrossRef](#)]
30. Wu, J.; Gao, X.J. A gridded daily observation dataset over China region and comparison with the other datasets. *Chin. J. Geophys.* **2013**, *56*, 1102–1111. (In Chinese with English Abstract) [[CrossRef](#)]
31. Zhou, B.; Xu, Y.; Wu, J.; Dong, S.; Shi, Y. Changes in temperature and precipitation extreme indices over China: Analysis of a high-resolution grid dataset. *Int. J. Climatol.* **2016**, *36*, 1051–1066. [[CrossRef](#)]
32. Kunkel, K.E.; Easterling, D.R.; Kristovich, D.A.; Gleason, B.; Stoecker, L.; Smith, R. Recent increases in US heavy precipitation associated with tropical cyclones. *Geophys. Res. Lett.* **2010**, *37*. [[CrossRef](#)]
33. Aryal, Y.N.; Villarini, G.; Zhang, W.; Vecchi, G.A. Long term changes in flooding and heavy rainfall associated with North Atlantic tropical cyclones: Roles of the North Atlantic Oscillation and El Niño–Southern Oscillation. *J. Hydrol.* **2018**, *559*, 698–710. [[CrossRef](#)]
34. Gao, T.; Wang, H. Trends in precipitation extremes over the Yellow River basin in North China: Changing properties and causes. *Hydrol. Process.* **2017**, *31*, 2412–2428. [[CrossRef](#)]
35. Matonse, A.H.; Frei, A.A. Seasonal Shift in the Frequency of Extreme Hydrological Events in Southern New York State. *J. Clim.* **2013**, *26*, 9577–9593. [[CrossRef](#)]
36. Marquardt Collow, A.B.; Bosilovich, M.G.; Koster, R.D. Large-Scale Influences on Summertime Extreme Precipitation in the Northeastern United States. *J. Hydrometeorol.* **2016**, *17*, 3045–3061. [[CrossRef](#)] [[PubMed](#)]
37. Li, R.C.; Zhou, W. Multiscale control of summertime persistent heavy precipitation events over South China in association with synoptic, intraseasonal, and low-frequency background. *Clim. Dynam.* **2015**, *45*, 1043–1057. [[CrossRef](#)]
38. Chen, Y.; Zhai, P. Mechanisms for concurrent low-latitude circulation anomalies responsible for persistent extreme precipitation in the Yangtze River Valley. *Clim. Dynam.* **2016**, *47*, 989–1006. [[CrossRef](#)]
39. Zhang, Q.; Zhang, W.; Lu, X.; Chen, Y.D. Landfalling tropical cyclones activities in the south China: Intensifying or weakening? *Int. J. Climatol.* **2012**, *32*, 1815–1824. [[CrossRef](#)]
40. Luo, M.; Leung, Y.; Graf, H.F.; Herzog, M.; Zhang, W. Interannual variability of the onset of the South China Sea summer monsoon. *Int. J. Climatol.* **2016**, *36*, 550–562. [[CrossRef](#)]
41. Gao, T.; Xie, L. Spatiotemporal changes in precipitation extremes over Yangtze River basin. China, considering the rainfall shift in the late 1970s. *Glob. Planet. Chang.* **2016**, *147*, 106–124. [[CrossRef](#)]

42. Zhang, Q.; Lai, Y.; Gu, X.; Shi, P.; Singh, V.P. Tropical Cyclonic Rainfall in China: Changing Properties, Seasonality, and Causes. *J. Geophys. Res. Atmos.* **2018**, *123*, 4476–4489. [[CrossRef](#)]
43. Li, M.; Guan, Z.; Jin, D.; Han, J.; Zhang, Q. Anomalous circulation patterns in association with two types of daily precipitation extremes over southeastern China during boreal summer. *J. Meteorol. Res.* **2016**, *30*, 183–202. [[CrossRef](#)]
44. Kao, H.; Yu, J. Contrasting eastern-Pacific and central-Pacific types of ENSO. *J. Clim.* **2009**, *22*, 615–632. [[CrossRef](#)]
45. Yu, J.Y.; Kao, H.Y. Decadal changes of ENSO persistence barrier in SST and ocean heat content indices: 1958–2001. *J. Geophys. Res. Atmos.* **2007**, *112*. [[CrossRef](#)]
46. An, S.; Wang, B. Mechanisms of locking of the El Niño and La Niña mature phases to boreal winter. *J. Clim.* **2001**, *14*, 2164–2176. [[CrossRef](#)]
47. Wang, B.; Zhang, Q. Pacific–east Asian teleconnection. Part II: How the Philippine Sea anomalous anticyclone is established during El Nino development. *J. Clim.* **2002**, *15*, 3252–3265. [[CrossRef](#)]
48. You, Q.; Kang, S.; Flügel, W.; Sanchez-Lorenzo, A.; Yan, Y.; Xu, Y.; Huang, J. Does a weekend effect in diurnal temperature range exist in the eastern and central Tibetan Plateau? *Environ. Res. Lett.* **2009**, *4*, 45202. [[CrossRef](#)]
49. Miao, C.; Sun, Q.; Borthwick, A.G.; Duan, Q. Linkage between hourly precipitation events and atmospheric temperature changes over China during the warm season. *Sci. Rep.* **2016**, *6*, 22543. [[CrossRef](#)]
50. Kendon, E.J.; Blenkinsop, S.; Fowler, H.J. When will we detect changes in short-duration precipitation extremes? *J. Clim.* **2018**, *31*, 2945–2964. [[CrossRef](#)]
51. Jiang, H.; Zipser, E.J. Contribution of tropical cyclones to the global precipitation from eight seasons of TRMM data: Regional, seasonal, and interannual variations. *J. Clim.* **2010**, *23*, 1526–1543. [[CrossRef](#)]



© 2019 by the authors. Licensee MDPI, Basel, Switzerland. This article is an open access article distributed under the terms and conditions of the Creative Commons Attribution (CC BY) license (<http://creativecommons.org/licenses/by/4.0/>).